CHEMISTRY

The missing link between zeolites and polyoxometalates

Guangmei Wang[1], Katharina V. Dorn[1], Stefanie Siebeneichler[1], Martin Valldor[2], Volodymyr Smetana[1], Anja-Verena Mudring[1,3]*

Copyright © 2022 The Authors, some rights reserved; exclusive licensee American Association for the Advancement of Science. No claim to original U.S. Government Works. Distributed under a Creative Commons Attribution NonCommercial License 4.0 (CC BY-NC).

Open framework materials such as zeolites and metalorganic frameworks are garnering tremendous interest because of their intriguing architecture and attractive functionalities. Thus, new types of open framework materials are highly sought after. Here, we present the discovery of completely new inorganic framework materials, where, in contrast to conventional inorganic open frameworks, the scaffold is not based on tetrahedral EO_4 (E = main group element) but octahedral MO_6 (M = transition metal) building blocks. These structural features place them closer to polyoxometalates than zeolites. The first representatives of this class of materials are $[(R)_{24}(NH_4)_{14}(PO(OH)_2)_6]\cdot[M_{134}(PO_3(OH,F))_{96}F_{120}]$ (M = Co, R = C_2Py = 1-ethylpyridinium and M = Ni, R = C_4C_1Py = 1-butyl-3-methylpyridinium) featuring interlinked fullerene-like nanosphere cavities. Having a transition metal building up the framework brings about interesting properties, for example, spin-glass behavior, and, with this particular topology, a hedgehog-like spin orientation.

INTRODUCTION

The Nobel Prize–winning discoveries of the carbon allotropes fullerenes (*1*, *2*) and graphene (*3*, *4*) are clear evidence that the topology generated through the connectivity of atoms has a massive influence on materials properties even of simple elements and can open up completely unimagined motifs. A class of compounds that traditionally has been in focus from the view of unique topologies are open framework materials such as zeolites. They not only exhibit enormous structural diversity (*5*) but also represent extremely demanded functional materials of high industrial relevance (*6*). Since the discovery of natural zeolites and the realization of their application potential, the class of open framework materials has continuously been expanded: metal-organic frameworks (*7*), covalent organic frameworks (*8*), and porous organic polymers (*9*). Many of these have generated subclasses of materials in their own right such as zeolitic imidazolium frameworks (*10*, *11*), a branch of hybrid inorganic-organic frameworks or (metal)-aluminophosphates (*12*), and a subgroup of inorganic open framework materials closely related to zeolites.

In terms of stability, purely inorganic framework materials are unique, which renders them most attractive for applications. Yet, practically all known inorganic open framework materials appear to be principally restricted to tetrahedral EO_4 (E = main group element) primary building units, most commonly silicate (SiO_4^{4-}) or phosphate (PO_4^{3-}) groups. Here, we report on unprecedented inorganic framework materials of composition $[(R)_{24}(NH_4)_{14}(PO(OH)_2)_6]\cdot[M_{134}(PO_3(OH,F))_{96}F_{120}]$ (M = Co, R = C_2Py = 1-ethylpyridinium and M = Ni, R = C_4C_1Py = 1-butyl-3-methylpyridinium; table S3) where, despite the present PO_4 groups, transition metal octahedral (MO_6) units exclusively build the framework. The framework extends uniformly and isotropically, resulting in the spherical shape of the cavities. The resultant architecture, albeit reminiscent of zeolites with their high structural symmetry and cavities, follows different building rules when compared to classical tetrahedral-based zeolite-type formations and involves the full spectrum of interconnection of Platonic polyhedra, such as edge-, face-, and corner-sharing. The new compounds may be best described as a hybrid between zeolites and polyoxometalates (POMs) (*13*–*21*). The latter are characterized by interconnected (MO_6) building blocks, but feature isolated polyanions rather than a framework structure. The fascinating new topology of $[(R)_{24}(NH_4)_{14}(PO(OH)_2)_6]\cdot[M_{134}(PO_3(OH,F))_{96}F_{120}]$ constructed from commonly encountered purely inorganic building blocks combining features of zeolites and POMs presents a noteworthy step in the evolution of a new class of open framework materials with desired properties and property combinations.

RESULTS AND DISCUSSION

Syntheses and structural characterization

The title compounds were synthesized following an ionothermal approach (*22*, *23*) using pyridinium hexafluorophosphate ionic liquids (ILs) as solvents, templating agents, mineralizer, and fluoride sources, all in one, in ionothermal reactions at temperatures ≤180°C [T_m(ILs) = 45° to 106°C]. Whereas cobalt(II) acetate tetrahydrate $Co(OAc)_2{\cdot}4\ H_2O$ was used as a metal source for compound **1**, nickel(II) chloride hexahydrate $NiCl_2{\cdot}6\ H_2O$ was used for compound **2**. For both, ammonium dihydrogen phosphate $(NH_4)H_2PO_4$ provided the phosphate groups. Boric acid was added to scavenge an excess of in situ generated hydrofluoric acid; however, it is not essential for the formation of the desired products. The use of ILs is key for the formation of these open framework materials as they act as a reaction medium, a mineralizer, and a templating agent. It is, however, interesting that Ni required its own IL to form the same framework structure, which could not be exchanged or substituted. We attribute this to the specific cation-IL interactions, which are different for different ions. The omission of traditional solvents

[1]Department of Materials and Environmental Chemistry, Stockholm University, Svante Arrhenius väg 16C, Stockholm 10691, Sweden. [2]Centre for Materials Science and Nanotechnology, Department of Chemistry, University of Oslo, Postbox 1033, Blindern, 0315 Oslo, Norway. [3]Department of Chemistry and iNANO, 253 Aarhus University, 8000 Aarhus C, Denmark.
*Corresponding author. Email: anja-verena.mudring@mmk.su.se

prevents any unwanted interactions such as competing interactions with a more coordinating solvent, avoiding the formation of denser phases.

A detailed synthesis description is given in the Supplementary Materials. Single-crystal x-ray diffraction was conducted for octahedrally shaped crystals of compound **1** (see Fig. 1, A and B, and table S2). The phase purity of the samples was confirmed by powder X-ray diffraction (see Fig. 1C and fig. S2) and infrared vibrational spectroscopy (see fig. S4).

The novel framework materials' crystal structure reveals a honeycomb spherical topology of the transition metal framework (Fig. 1, D to F). Octahedral coordination of metal cations by oxygen in the basic building (MO_6) units leads to considerably different framework formation principles compared to the classical silicates or phosphates with tetrahedral building units. The classical Pauling rules (*24*) are violated, as the primary (MO_6) building units share not only vertices but also edges and faces (Fig. 1E), which results in shorter polyhedral-centering cation-cation distances, which, in turn, is expected to reduce the stability. However, the centers of gravity come closer in edge- and face-sharing tetrahedral, compared to octahedral and, in consequence, the destabilization is less in octahedral formations. In addition, the scaffold of interconnected octahedral is decorated with isolated vertex-sharing PO_3(OH,F) groups that bring about additional stabilization. Note that these tetrahedral groups are neither building up the framework nor connected as in the inorganic framework materials known to date. An interesting structural relation to POMs exists, where the incorporation of EO_4 groups can be observed, e.g., in the Keggin anion (*25*, *26*). In the present case, the PO_3(OH,F) groups help reduce the charge of the network. The remaining charge is compensated by cations located in the framework cavities (vide infra).

While natural zeolites are mostly aluminosilicates, synthetic zeolites allow the incorporation of a larger number of *p* elements and some *s* and *d* metals on the tetrahedrally coordinated sites (*27*, *28*). Involvement of independent octahedral transition metal–containing units (0D, 1D, or 2D) with different connectivities is also possible (*29*); however, they always require tetrahedral linkers such as phosphate groups to form a 3D carcass. The phosphate groups here do not participate in the generation of the network. Their role is to stabilize the octahedral honeycomb sphere sharing the O vertices with the octahedra from the concave side enforcing the construction and removing strain.

Despite a very limited number of pores (which comes from the high symmetry), they provide ~5100 $Å^3$ of solvent-accessible space that is equal to a total of 33% of the unit cell volume. The framework density (FD) of 14.8 corresponds to 8.7 octahedral (Co or Ni) and 6.1 tetrahedral (P) centers per 1000 $Å^3$. Compared to values ranging from 12 to 20 for structures with extensive large pore volumes, this FD is appreciably low (*30*). The 12-atom pore openings of which 8 are octahedrally coordinated are in the shape of a butterfly (Fig. 1E). They are comparatively small with respect to the cavity size. The solvent-accessible opening is practically round with a maximum diameter of 5.2 Å but slightly irregular due to alternating octahedral F^- versus OH^- bridging ligands (fig. S3). This suggests that the maximum accessible opening of 4.1 × ~3.2 Å is potentially helpful for the selective solvents or gas sorption. The irregular shape of the pore opening is large enough for all small molecules (N_2, CO_2, and H_2O) but may already be problematic for even small alkenes, e.g.,

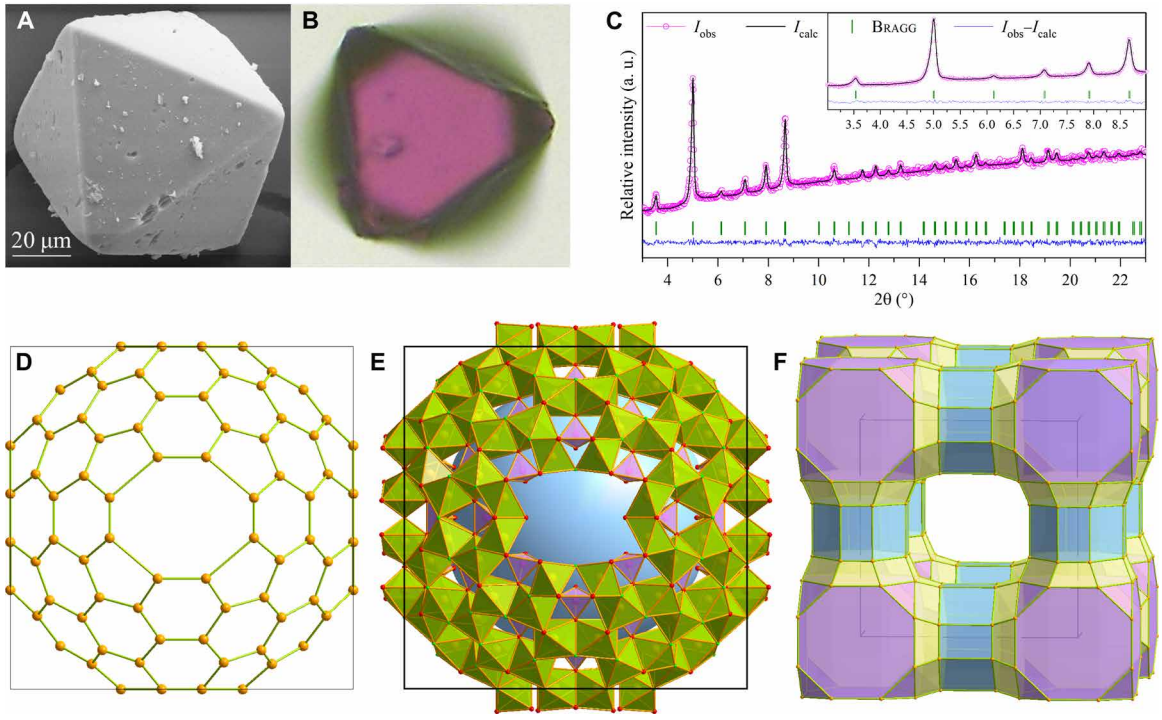

Fig. 1. Synthesis and structural aspects of compound 1. Octahedrally shaped single crystals of compound **1** (Co) as observed from (**A**) scanning electron microscopy and (**B**) optical microscopy. Le Bail (*47*) powder profile-fitting for compound **1** from 3° to 23° 2θ (**C**) as well as a close-up view ranging from 3° to 9° 2θ (C, inset). Representation of the cubic crystal structure of the compounds emphasizing the metal network (**D**), the spherical packing of the polyhedral [transition metal octahedra in green, PO_3(OH,F) tetrahedra in mauve] (**E**), and the cage assembly (**F**).

ethane/ethylene, requiring a ~4-Å pore opening (*31*). To evaluate the accessible surface area, we carried out Brunauer-Emmett-Teller measurements. This resulted in a surface area of 147.0 m^2/g, a total pore volume of 0.18 cm^3/g, and a micropore volume of 0.035 cm^3/g. These values are typical for microporous zeolitic materials (*32*), although higher values can be achieved for extra-large pore zeolites (*33*).

The smaller cavities (Fig. 1F, purple) are in the form of truncated cubes (six octagonal and eight trigonal faces) and form, together with the octagonal prismatic connectors, a separate system of channels well isolated from the central cavity. These channels are accessible for water or other small solvents as supported by the results of thermal investigations (see Fig. 2 and fig. S5).

The network bears a negative charge of 44−/formula unit (see table S2). This charge is, in part (24+), compensated by IL cations ($[C_2Py]^+$ for the Co compound and $[C_4C_1Py]^+$ for the Ni compound), while the rest belong to disordered NH_4^+ cations located in the cavities (see also fig. S4).

In line with the honeycomb topology observed in the most abundant modifications of carbon, nature may allow crystal structures to assume monolayer ball-like constructs (*1*, *2*). Considering inorganic transition metal salts, spherical topologies in extended solids have not been observed to date. The closest structural analogies come from the POM chemistry including isolated (0D) POM cluster assemblies with Keplerate architecture (*34*) or a family of zeolitic octahedral metal oxides, the so-called ZOMOs (*13*). In particular, ε-Keggin POM clusters with the help of additional octahedral linkers may extend in a variety of topologies including pseudo-spherical (*35*–*38*). It is worth mentioning that all topologies in this family of materials also referred to as POMzites (*36*) are the result of two types of building units—large POM clusters and smaller linkers typically of different nature. The latter is clearly lacking in our structures.

The presented new open framework materials also bear analogies to fundamental topologies with nonclassical fullerenes, particularly those based on 8-circulene (sumanene) (*39*)—flower-like aromatic molecules with octagonal core and petals consisting of five to seven rings (*40*): The Co_{152} sphere of 25 Å in diameter consists of six edge-sharing flowers [8:(5,6)$_4$] complemented by 8 "naphthalene" fragments (6_2) (Fig. 1, D to F, and fig. S3). The spheres, in turn, condensate through octagonal faces along all main crystallographic axes. The openings (octagon fused with four pentagons; fig. S3) show similarity to the tetrahedral gallophosphate cloverite (*41*).

Thermal properties

Compounds **1** and **2** remain stable and structurally intact up to 320°C, as confirmed by TG (thermogravimetry) and powder X-ray diffraction measurements (fig. S5). The weight loss at that temperature corresponds to approximately one water molecule per Co atom, which is in good agreement with the solvent-accessible volume accounting also for IL cations. We evidenced that. up to this temperature, water can be reversibly taken up and released without structural changes of the framework. Simultaneous mass spectrometry and thermogravimetric analysis show for **1** that upon further heating ammonium, hydrophosphate and alkyl chains of the IL cations ($T \geq 118$°C) are released. At temperatures ≥423°C $[C_2Py]^+$, the aromatic rings and HF are lost and lastly the dense metal phosphate, $Co_3(PO_4)_2$, forms.

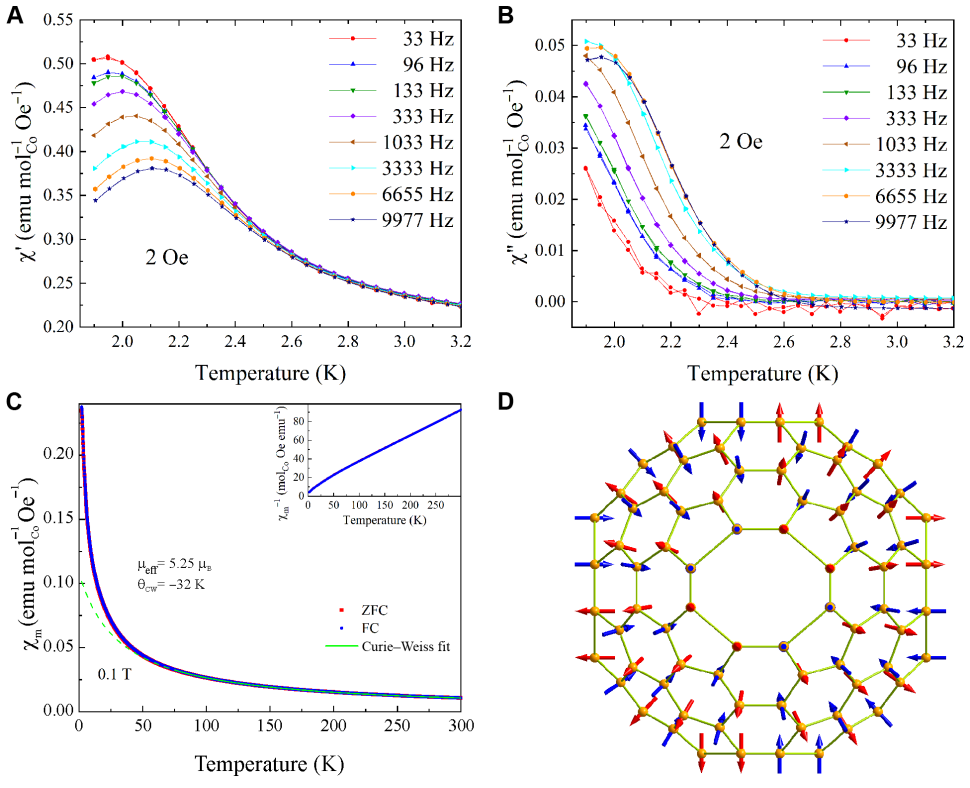

Fig. 2. Magnetic properties of compound 1. Real (**A**) and imaginary (**B**) part of the magnetic susceptibility of compound **1** (Co), as measured in an AC field at different frequencies. (**C**) Temperature-dependent magnetic susceptibility and inverse susceptibility (inset) of compound **1** (Co). (**D**) Representation of a local hedgehog antiferromagnetic spin ordering.

Magnetic properties

Ultraviolet-visible (UV-vis) spectroscopy unambiguously shows the presence of Ni^{2+} and Co^{2+} in **1** and **2**, respectively (fig. S7). The oxidation state of Co was further confirmed with X-ray photoelectron spectroscopy (XPS) measurements (fig. S10). With an unprecedented spherical topology of the magnetic lattice evoked by the divalent transition metal cations, what kind of magnetic properties can be expected? For example, the Keplerates (*34*) exhibit magnetic frustration due to a triangular arrangement of magnetic atoms on the surface of the isolated (!) spheres formed by the magnetically active ion. Magnetic susceptibility data confirm for **1** and **2** the presence of divalent Ni and Co with an antiferromagnetic ground state in the high-temperature regime (Fig. 2C and figs. S7 and S8). Low-temperature measurements reveal the magnetic frustration and spin-glass–like behavior. Measurements at low temperatures ($1.9 < T < 3$ K) in an alternating external magnetic field indicate the formation of magnetic domains with short-range spin ordering. The strong temperature shift with field frequency and the large magnetic energy loss, i.e., the imaginary signal part is ~10% of the real part, allow us to discern that the magnetic domains must be relatively large (Fig. 2, A and B), likely the size of the spheres composed of the TM centers (Fig. 1D). It is possible that the spins are oriented perpendicular to the surface of the sphere. This local spin ordering would allow retaining the threefold axis along the cubic space diagonal and, hence, be crystallographically compatible, resulting in a hedgehog spin ordering (Fig. 2D).

Ionothermal synthesis allowed us to obtain $[(R)_{24}(NH_4)_{14}(PO(OH)_2)_6]\cdot[M_{134}(PO_3(OH,F))_{96}F_{120}]$ (M = Co, R = C_2Py = 1-ethylpyridinium and M = Ni, R = C_4C_1Py = 1-butyl-3-methylpyridinium). ILs are key to the formation of this novel class of inorganic open framework materials as they help to avoid the formation of dense phases. Structurally, the new compounds represent a new class of their own. They could be understood as a hybrid between zeolites and POMs. Unlike in any known open framework structure, the scaffold is exclusively formed by transition metal octahedral (MO_6) units. These unprecedented primary building units lead to considerably different framework formation principles compared to the classical inorganic open framework structures with their tetrahedral building units and bring about new functionalities. In the present case, interlinkage of (MO_6) octahedra leads to a low-density, highly porous framework with ball-like spheres that are reminiscent of fullerenes. Decorating these spheres with the magnetic moments brought about from the magnetic transition metal ions leads to a spin structure that reminds us of a hedgehog.

MATERIALS AND METHODS

Reagents and syntheses

Suppliers and purities of all starting materials are listed in table S1. The reactions for the title compounds **1** (Co) and **2** (Ni) were conducted as follows:

1: All starting materials, 1-ethylpyridinium hexafluorophosphate $[C_2Py][PF_6]$ (253 mg, 0.999 mmol), cobalt(II) acetate tetrahydrate $Co(OAc)_2 \cdot 4\ H_2O$ (227 mg, 0.911 mmol), ammonium dihydrogen phosphate $(NH_4)H_2PO_4$ (124 mg, 1.078 mmol), and boric acid H_3BO_3 (≤16.5 mg, ≤0.267 mmol), were mixed at a molar ratio of 3.7:3.4:4.0:0.0 to 1.0, ground in an agate mortar, and placed in a 15-ml Teflon vessel, which was closed by its screwing cap. The reaction was conducted in a drying oven with a heating rate of 1°C min^{-1}, an isothermal step at 115°C [T_m(IL) = 106°C] for 2 hours, a maximum reaction temperature of 180°C [$T_m(Co(OAc)_2 \cdot 4\ H_2O)$ = 140°C, $T_d(Co(OAc)_2 \cdot 4\ H_2O)$ = 180°C] for 7 days, and a cooling rate of 0.03°C min^{-1} (2.08°C $hour^{-1}$) according to the heating scheme shown in fig. S1. The lilac raw product was purified by washing with 30 ml of ethanol and further 30 ml of deionized water. After filtration, the product was dried in air and a pink microcrystalline powder was received. Besides the abovementioned IL, the synthesis can also be performed with 1-butyl- or 1-hexylpyridinium and 1-butyl-*x*-methylpyridinium (x = 2, 3, and 4) hexafluorophosphate in a molar ratio ranging from 3.2 to 3.8. Smaller batch sizes and the use of the butylpyridinium hexafluorophosphate promote a better crystal growth (see Fig. 1, A and B).

2: A mixture of the reactants 1-butyl-3-methylpyridinium hexafluorophosphate (253 mg, 0.857 mmol), nickel(II) chloride hexahydrate $NiCl_2 \cdot 6\ H_2O$ (129 mg, 0.543 mmol), ammonium dihydrogen phosphate $(NH_4)H_2PO_4$ (124 mg, 1.078 mmol), and boric acid H_3BO_3 (≤16.5 mg, ≤0.267 mmol) at a molar ratio of 3.2:2.0:4.0:0.0 to 1.0 was ground and heated to 170°C [T_m(IL) = 52°C] in a 15-ml Teflon container, which was closed by its screwing cap, with a heating rate of 1°C min^{-1} and a cooling rate of 0.03°C min^{-1} (1.81°C $hour^{-1}$) as shown in fig. S1. After washing with 30 ml of deionized water, filtration, and drying in air, a yellow-green microcrystalline powder was obtained.

Methods

Single-crystal x-ray diffraction

The crystal structural measurement of compound **1** (Co, see table S2) was carried out on a Bruker Venture diffractometer equipped with a Photon 100 complementary metal-oxide semiconductor detector and an IμS microfocus source using Mo K_α radiation (λ = 0.71073 Å) at room temperature. Intensity data of reflections were integrated using SAINT within the APEX3 software package (*42*). SADABS (*43*) was used for the absorption corrections. The crystal structure solution was performed by direct methods using SHELXT (*44*). SHELXL-2013 (*45*) was used for the subsequent difference Fourier analyses and least squares refinement. All nonhydrogen atoms were refined anisotropically. The disordered solvent contributions have been estimated with the PLATON SQUEEZE tool (*46*).

Powder x-ray diffraction

Intensity datasets for powder x-ray diffraction of both title compounds were recorded by using a Panalytical X'Pert PRO diffractometer in Bragg-Bretano geometry with Cu K_α radiation (λ_1 = 1.54059 Å and λ_2 = 1.54443 Å) and a PW3015/20 X'Celerator at room temperature. The Le Bail (*47*) profile matchings of the powder diffractograms performed with FullProf (*48*, *49*) and WinPLOTR (*50*) are shown in Fig. 1C and fig. S2.

Magnetic measurements

The magnetic properties of both title compounds were measured on a Physical Properties Measurement System from Quantum Design (USA). The Vibrating Sample Magnetometer (VMS) option was used for temperature and field dependence in static (DC) fields at 0.1 T and up to 7 T, respectively. Polycrystalline samples were loaded into polypropylene capsules, which were mounted in a brass sample holder. The magnetization signals of both title compounds are magnitudes larger than that of the empty sample holder. Therefore, no diamagnetic corrects were applied. Frequency-dependent magnetization measurements were collected using the AC Measurement System option with a constant amplitude of 2 Oe and frequencies

from 33 to 9977 Hz at low temperatures. For these, a polycrystalline sample was placed into a gelatin capsule, which was mounted in a plastic straw. To prevent the sample from moving during measurements, the capsule was filled up with quartz wool.

Thermal analysis

TG (see fig. S7) for both title compounds **1** (Co, 3.898 mg) and **2** (Ni, 1.239 mg) was conducted with a PerkinElmer TGA 7 in alumina pans under air flow with heating rates of 3°C min^{-1} (Co) and 10°C min^{-1} (Ni). TG analysis and mass spectrometry (see fig. S3) measurements were conducted with a Discovery TGA (TA Instruments, Sweden) coupled to an Omnistar GSD 320 mass spectrometer (Pfeiffer Vacuum, Sweden). Compound **1** (Co, 6.19744 mg) was, therefore, heated to 900°C with a ramp of 5°C min^{-1} after an isothermal step at 30°C for 30 min by using a high-temperature platinum pan and argon gas.

Vibrational spectroscopy

Infrared spectra (see fig. S8) of the title compounds **1** (Co) and **2** (Ni) were recorded on a Bruker Alpha-P spectrometer (Bruker Nordic, Sweden) equipped with a single-reflection diamond ATR accessory (Platinum ATR) in a range of 400 to 4000 cm^{-1} at room temperature.

UV-vis spectroscopy

The spectra of powders of both title compounds (see fig. S9) were recorded at room temperature with an Agilent Technologies Cary 5000 UV-vis–NIR spectrophotometer (Agilent, USA) using an internal diffuse-reflectance accessory (Praying Mantis, Harrick, USA) in a range of 350 to 800 nm. Optical-grade barium sulfate ($BaSO_4$) was used as a reference.

Gas adsorption analysis

N_2 gas adsorption/desorption isotherms were recorded using a Micromeritics ASAP 2020 surface area analyzer at pressures of 0 to 101 kPa. The samples were prepared by heating to 523 K under high dynamic vacuum (1×10^{-4} Pa) for 6 hours. The N_2 uptake at 77 K was determined using a liquid N_2 bath as the temperature control medium (fig. S11).

SUPPLEMENTARY MATERIALS

Supplementary material for this article is available at https://science.org/doi/10.1126/sciadv.add9320

REFERENCES AND NOTES

1. H. W. Kroto, J. R. Heath, S. C. O'Brien, R. F. Curl, R. E. Smalley, C_{60}: Buckminsterfullerene. *Nature* **318**, 162–163 (1985).
2. H. W. Kroto, The stability of the fullerenes C*n*, with *n* = 24, 28, 32, 36, 50, 60 and 70. *Nature* **329**, 529–531 (1987).
3. K. S. Novoselov, A. K. Geim, S. V. Morozov, D. Jiang, Y. Zhang, S. V. Dubonos, I. V. Grigorieva, A. A. Firsov, Electric field effect in atomically thin carbon films. *Science* **306**, 666–669 (2004).
4. A. K. Geim, K. S. Novoselov, The rise of graphene. *Nat. Mater.* **6**, 183–191 (2007).
5. C. Baerlocher, L. B. McCusker, D. H. Olson, *Atlas of Zeolite Framework Types*. (Elsevier, 2007).
6. M. E. Davis, Ordered porous materials for emerging applications. *Nature* **417**, 813–821 (2002).
7. Q. Wang, D. Astruc, State of the art and prospects in Metal–Organic Framework (MOF)-based and MOF-derived nanocatalysis. *Chem. Rev.* **120**, 1438–1511 (2020).
8. K. Geng, T. He, R. Liu, S. Dalapati, K. T. Tan, Z. Li, S. Tao, Y. Gong, Q. Jiang, D. Jiang, Covalent organic frameworks: Design, synthesis, and functions. *Chem. Rev.* **120**, 8814–8933 (2020).
9. T. Zhang, G. Xing, W. Chen, L. Chen, Porous organic polymers: A promising platform for efficient photocatalysis. *Mater. Chem. Front.* **4**, 332–353 (2020).
10. J. C. Tan, T. D. Bennett, A. K. Cheetham, Chemical structure, network topology, and porosity effects on the mechanical properties of zeolitic imidazolate frameworks. *Proc. Natl. Acad. Sci. U.S.A.* **107**, 9938–9943 (2010).
11. B. Chen, Z. Yang, Y. Zhu, Y. Xia, Zeolitic imidazolate framework materials: Recent progress in synthesis and applications. *J. Mater. Chem. A* **2**, 16811–16831 (2014).
12. C. Zheng, Y. Li, J. Yu, Database of open-framework aluminophosphate structures. *Sci. Data* **7**, 107 (2020).
13. L. Vilà-Nadal, L. Cronin, Design and synthesis of polyoxometalate-framework materials from cluster precursors. *Nat. Rev. Mater.* **2**, 17054 (2017).
14. H. N. Miras, L. Vilà-Nadal, L. Cronin, Polyoxometalate based open-frameworks (POM-OFs). *Chem. Soc. Rev.* **43**, 5679–5699 (2014).
15. M. J. Turo, L. Chen, C. E. Moore, A. M. Schimpf, Co^{2+}-linked $[NaP_5W_{30}O_{110}]^{14-}$: A redox-active metal oxide framework with high electron density. *J. Am. Chem. Soc.* **141**, 4553–4557 (2019).
16. L. Chen, M. J. Turo, M. Gembicky, R. A. Reinicke, A. M. Schimpf, Cation-controlled assembly of polyoxotungstate-based coordination networks. *Angew. Chem. Int. Ed.* **59**, 16609–16615 (2020).
17. K. Suzuki, Y. Kikukawa, S. Uchida, H. Tokoro, K. Imoto, S.-i. Ohkoshi, N. Mizuno, Three-dimensional ordered arrays of 58×58×58 $Å^3$ hollow frameworks in ionic crystals of M_2Zn_2-substituted polyoxometalates. *Angew. Chem. Int. Ed.* **51**, 1597–1601 (2012).
18. T. Kotabe, Y. Ogasawara, K. Suzuki, S. Uchida, N. Mizuno, K. Yamaguchi, Porous cubic cesium salts of silicododecatungstate(molybdate)/borododecatungstate blends: Synthesis and molecular adsorption properties. *Inorg. Chem.* **57**, 8821–8830 (2018).
19. T. Auvray, E. M. Matson, Polyoxometalate-based complexes as ligands for the study of actinide chemistry. *Dalton Trans.* **49**, 13917–13927 (2020).
20. L. E. VanGelder, A. M. Kosswattaarachchi, P. L. Forrestel, T. R. Cook, E. M. Matson, Polyoxovanadate-alkoxide clusters as multi-electron charge carriers for symmetric non-aqueous redox flow batteries. *Chem. Sci.* **9**, 1692–1699 (2018).
21. S. G. Mitchell, C. Streb, H. N. Miras, T. Boyd, D.-L. Long, L. Cronin, Face-directed self-assembly of an electronically active Archimedean polyoxometalate architecture. *Nat. Chem.* **2**, 308–312 (2010).
22. R. E. Morris, Ionothermal synthesis—Ionic liquids as functional solvents in the preparation of crystalline materials. *Chem. Commun.* **21**, 2990–2998 (2009).
23. M. Li, A. Verena-Mudring, New developments in the synthesis, structure, and applications of borophosphates and metalloborophosphates. *Cryst. Growth Des.* **16**, 2441–2458 (2016).
24. L. Pauling, The principles determining the structure of complex ionic crystals. *J. Am. Chem. Soc.* **51**, 1010–1026 (1929).
25. J. F. Keggin, The structure and formula of 12-phosphotungstic acid. *Proc. R. Soc. A.* **144**, 75–100 (1934).
26. J. B. Martin, D. M. Doty, Determination of inorganic phosphate. *Anal. Chem.* **21**, 965–967 (1949).
27. T. E. Gier, G. D. Stucky, Low-temperature synthesis of hydrated zinco(beryllo)-phosphate and arsenate molecular sieves. *Nature* **349**, 508–510 (1991).
28. P. Feng, X. Bu, G. D. Stucky, Hydrothermal syntheses and structural characterization of zeolite analogue compounds based on cobalt phosphate. *Nature* **388**, 735–741 (1997).
29. G. Wang, M. Valldor, K. V. Dorn, M. Wilk-Kozubek, V. Smetana, A.-V. Mudring, Ionothermal synthesis enables access to 3D open framework manganese phosphates containing extra-large 18-ring channels. *Chem. Mater.* **31**, 7329–7339 (2019).
30. G. O. Bnmner, W. M. Meier, Framework density distribution of zeolite-type tetrahedral nets. *Nature* **337**, 146–147 (1989).
31. Z. Bao, J. Wang, Z. Zhang, H. Xing, Q. Yang, Y. Yang, H. Wu, R. Krishna, W. Zhou, B. Chen, Q. Ren, Molecular sieving of ethane from ethylene through the molecular cross-section size differentiation in gallate-based metal–organic frameworks. *Angew. Chem. Int. Ed. Engl.* **57**, 16020–16025 (2018).
32. M. Baninaam, S. A. Hosseini, A. R. Abbasian, Isothermal study of asphaltene adsorption over 4A, 13X, ZSM-5, clinoptilolite zeolites, and phoslock. *Appl. Petrochem. Res.* **10**, 49–54 (2020).
33. A. Corma, M. J. Díaz-Cabañas, J. Jiang, M. Afeworki, D. L. Dorset, S. L. Soled, K. G. Strohmaier, Extra-large pore zeolite (ITQ-40) with the lowest framework density containing double four- and double three-rings. *Proc. Natl. Acad. Sci. U.S.A.* **107**, 13997–14002 (2010).
34. A. Müller, A. M. Todea, J. van Slageren, M. Dressel, H. Bögge, M. Schmidtmann, M. Luban, L. Engelhardt, M. Rusu, Triangular geometrical and magnetic motifs uniquely linked on a spherical capsule surface. *Angew. Chem. Int. Ed.* **44**, 3857–3861 (2005).
35. J. Wang, Q. Zhu, Z. Zhang, M. Sadakane, Y. Li, W. Ueda, Zeolitic octahedral metal oxides with ultra-small micropores for C_2 hydrocarbon separation. *Angew. Chem. Int. Ed.* **60**, 18328–18334 (2021).
36. T. Boyd, S. G. Mitchell, D. Gabb, D.-L. Long, Y.-F. Song, L. Cronin, POMzites: A family of zeolitic polyoxometalate frameworks from a minimal building block library. *J. Am. Chem. Soc.* **139**, 5930–5938 (2017).
37. Z. Zhang, Q. Zhu, M. Sadakane, T. Murayama, N. Hiyoshi, A. Yamamoto, S. Hata, H. Yoshida, S. Ishikawa, M. Hara, W. Ueda, A zeolitic vanadotungstate family with structural diversity and ultrahigh porosity for catalysis. *Nat. Commun.* **9**, 3789 (2018).
38. D. Liu, Y. Lu, H.-Q. Tan, W.-L. Chen, Z.-M. Zhang, Y.-G. Li, E.-B. Wang, Polyoxometalate-based purely inorganic porous frameworks with selective adsorption and oxidative catalysis functionalities. *Chem. Commun.* **49**, 3673–3675 (2013).

39. H. Sakurai, T. Daiko, T. Hirao, A synthesis of sumanene, a fullerene fragment. *Science* **301**, 1878 (2003).
40. B. Szefler, M. V. Diudea, Quantum-mechanical calculations on molecular substructures involved in nanosystems. *Molecules* **19**, 15468–15506 (2014).
41. M. Estermann, L. B. McCusker, C. Baerlocher, A. Merrouche, H. Kessler, A synthetic gallophosphate molecular sieve with a 20-tetrahedral-atom pore opening. *Nature* **352**, 320–323 (1991).
42. APEX3 and SAINT. Bruker AXS Inc., Madison, Wisconsin, USA (2015).
43. L. Krause, R. Herbst-Irmer, D. Stalke, An empirical correction for the influence of low-energy contamination. *J. Appl. Cryst.* **48**, 1907–1913 (2015).
44. G. M. Sheldrick, *SHELXT* - Integrated space-group and crystal-structure determination. *Acta Cryst.* **A71**, 3–8 (2015).
45. G. M. Sheldrick, Crystal structure refinement *with SHELXL*. *Acta Cryst.* **C71**, 3–8 (2015).
46. A. L. Spek, *PLATON* SQUEEZE: A tool for the calculation of the disordered solvent contribution to the calculated structure factors. *Acta Cryst.* **C71**, 9–18 (2015).
47. A. Le Bail, Whole powder pattern decomposition methods and applications: A retrospection. *Powder Diffr.* **20**, 316–326 (2005).
48. J. Rodríguez-Carvajal, Recent advances in magnetic structure determination by neutron powder diffraction. *Phys. Rev. B Condens. Matter* **192**, 55–69 (1993).
49. J. Rodriguez-Carvajal, Commission on powder diffraction (IUCr). *Newsletter* **26**, 12–19 (2001).
50. T. Roisnel, J. Rodriguez-Carvajal, in *Materials Science Forum. Proceedings of the European Powder Diffraction Conf. (EPDIC 7)*. (Citeseer, 2001).
51. D. Lin-Vien, N. B. Colthup, W. G. Fateley, J. G. Grasselli, *The Handbook of Infrared and Raman Characteristic Frequencies of Organic Molecules* (Elsevier, 1991).
52. A. Larrañaga, J. L. Mesa, J. L. Pizarro, R. Olazcuaga, F. Guillen, M. I. Arriortua, T. Rojo, Structural, luminescent and magnetic studies of Mn(HPO4).3H2O. *J. Phys. IV* **123**, 241–244 (2005).
53. V. Koleva, V. Stefov, A. Cahil, M. Najdoski, B. Šoptrajanov, B. Engelen, H. D. Lutz, Infrared and Raman studies of manganese dihydrogen phosphate dihydrate, $Mn(H_2PO_4)_2{\cdot}2H_2O$. I: Region of the vibrations of the phosphate ions and external modes of the water molecules. *J. Mol. Struct.* **917**, 117–124 (2009).
54. M. Weil, E. J. Baran, R. K. Kremer, E. Libowitzky, Synthesis, crystal structure, and properties of $Mn(PO_3F)(H_2O)_2$. *Z. Anorg. Allg. Chem.* **641**, 184–191 (2015).
55. F. A. Miller, C. H. Wilkins, Infrared spectra and characteristic frequencies of inorganic ions. *Anal. Chem.* **24**, 1253–1294 (1952).
56. J. Weidlein, U. Müller, K. Dehnicke, *Schwingungsfrequenzen I—Hauptgruppenelemente* (Georg Thieme Verlag, ed. 1, 1981).
57. M. Klähn, G. Mathias, C. Kötting, M. Nonella, J. Schlitter, K. Gerwert, P. Tavan, IR spectra of phosphate ions in aqueous solution: Predictions of a DFT/MM approach compared with observations. *J. Phys. Chem. A* **108**, 6186–6194 (2004).
58. W. Jastrzębski, M. Sitarz, M. Rokita, K. Bułat, Infrared spectroscopy of different phosphates structures. *SAA* **79**, 722–727 (2011).
59. Y. Lai, X. Liang, G. Yin, S. Yang, J. Wang, H. Zhu, H. Yu, Infrared spectra of iron phosphate glasses with gadolinium oxide. *J. Mol. Struct.* **1004**, 188–192 (2011).
60. G. Socrates, *Infrared and Raman Characteristic Group Frequencies—Tables and Charts* (John Wiley & Sons, Ltd., ed. 3, 2001).

Acknowledgments: We thank B. Förtsch (research group of D. Gudat, Institute of Inorganic Chemistry, University of Stuttgart, Stuttgart, Germany) for elemental analysis, F. C. Goerigk for the electron microprobe measurements, S. Kunkel for operating the hot gas extraction (research group of R. Niewa, Institute of Inorganic Chemistry, University of Stuttgart, Stuttgart, Germany), and A. H. Mamakhel (Department of Chemistry and iNano, Aarhus University, Langelandsgade 140, Aarhus 8000, Denmark) for XPS measurements. **Funding:** This research is funded, in part, by the Swedish Foundation for Strategic Research (SSF) within the Swedish national graduate school in neutron scattering (SwedNess). This research was supported, in part, through the Göran Gustafsson prize by the Royal Swedish Academy of Science to A.-V. M. and by the Swedish Research Council (Vetenskapsrådet, VR) through grant 2016-05405 as well as through the Aarhus University Research Foundation (AUFF).
Author contributions: A.-V.M. conceived the experiment. G.W., S.S., K.V.D., V.S., and M.V. analyzed and interpreted data. G.W., S.S., and K.V.D. prepared the samples. V.S., S.S., K.V.D., M.V., and A.-V.M. wrote the manuscript. **Competing interests:** The authors declare that they have no competing interests. **Data and materials availability:** All data needed to evaluate the conclusions in the paper are present in the paper and/or the Supplementary Materials. Related crystallographic information has been deposited with the Cambridge Structural Database and can be downloaded free of charge from www.ccdc.cam.ac.uk/. Accession code: CCDC-1971845.

Submitted 13 July 2022
Accepted 27 September 2022
Published 16 November 2022
10.1126/sciadv.add9320